Supporting Information for:

Next Generation Ultrafiltration Membranes Enabled by Block Polymers

Nicholas Hampu[‡], Jay R. Werber[†], Wui Yarn Chan[†], Elizabeth C. Feinberg[†], and Marc A. Hillmyer[†]*

[†]*Department of Chemistry, University of Minnesota, Minneapolis, Minnesota 55455*

[‡]*Department of Chemical Engineering and Materials Science, University of Minnesota Minneapolis, Minnesota 55455*

*Corresponding author (e-mail: hillmyer@umn.edu)

Derivation of Water Permeability Equation for Membranes with Tortuous Pores

Mesoporous membranes are commonly modeled as an array of parallel capillaries, with the water permeability estimated using the Hagen-Poiseuille (H-P) equation. In most cases, the pores are assumed to be cylindrical and vertical, resulting in the following equation for the water permeability, A, defined as the volumetric flux of water (J_w) normalized to the applied pressure gradient (ΔP) with units of L m^{-2} h^{-1} bar^{-1}:

$$A = \frac{J_w}{\Delta P} = \frac{\varepsilon r_p^2}{8\mu\delta_m} \text{ (for vertical pores)} \quad \text{(S1)}$$

The water permeability is calculated as a function of selective layer thickness (δ_m), pore radius (r_p), volumetric porosity (ε), and solution viscosity (μ). In most cases, pore radius is assumed to be uniform, although pore size distributions can be incorporated as well.

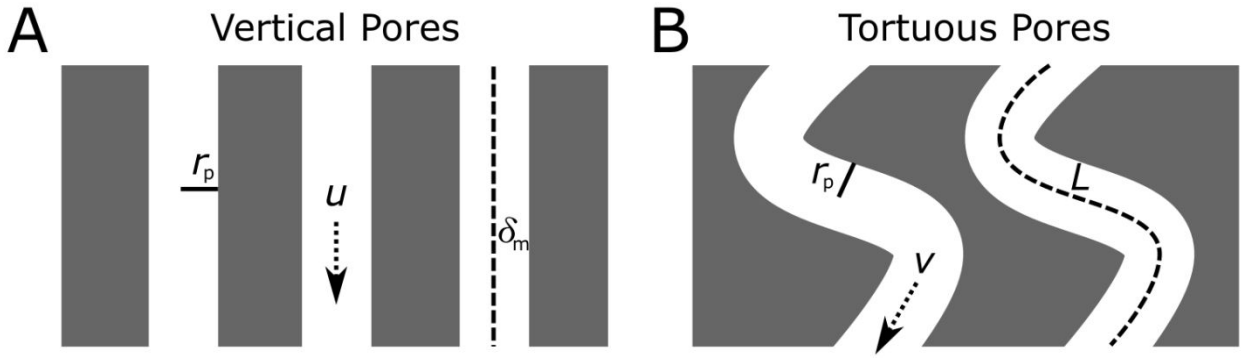

Figure S1. Schematic showing parallel arrays of (A) vertical pores and (B) tortuous pores, where both systems have the same selective layer thickness (δ_m), pore radius (r_p), and porosity (ε). The tortuous pores have a total pore length, L. Water flows through pores in the two systems at average velocities u and v, respectively. Note that the number of tortuous pores is fewer than for vertical pores for an equivalent volumetric porosity.

The pores of block polymer membranes (and other membranes) can include significant tortuosity (τ), defined as:

$$\tau = L/\delta_m \quad \text{(S2)}$$

where L is the pore length (Figure S1). Tortuosity values are greater than one in double gyroid and disordered morphologies, and can be greater than one in all morphologies by discontinuous grain boundaries or imperfect alignment. The effect of tortuosity can be incorporated directly into the water permeability equation (1). In the block polymer membrane literature, tortuosity has, we believe, erroneously been included in a modified H-P equation with a $1/\tau$ dependence. As derived in general fashion for the pressure drop in porous media by Epstein, tortuosity impacts the permeability in the H-P equation with a $1/\tau^2$ dependence, which leads to eq.1 in the main manuscript:

$$A = \frac{\varepsilon r_p^2}{8\tau^2\mu\delta_m} \quad \text{(1)}$$

The derivation by Epstein states that the increased pore length stemming from tortuosity has two effects: (1) decreasing the pressure gradient that drives flow, and (2) increasing the fluid velocity such that the average velocity in the capillary (v) exceeds that of the average interstitial axial velocity (u), which is equivalent to the capillary velocity for vertical pores. Combined, these two effects lead to the $1/\tau^2$ dependence. A key conceptual difference with the Epstein derivation is that the two main factors that drive the $1/\tau^2$ dependence include (1) the decreased pressure gradient and (2) a decreased number of pores for a constant porosity. This second factor increases velocity at fixed flux as in the Epstein derivation, but is more physically comprehensible.

Membrane water permeability is determined from the pure water flux, J_w, and the pressure drop, ΔP:

$$A = \frac{J_w}{\Delta P} \tag{S3}$$

The water flux is determined relative to the whole membrane surface area (a), including non-porous regions. For an array of uniform pores, the water flux is simply the product of the capillary velocity and the cross-sectional area of the pores (a_p), as determined in the normal direction from the pore walls:

$$J_w = v a_p \tag{S4}$$

For an array of cylindrical pores, the cross-sectional area is related to the total number of pores (n_p) and the total pore area (a):

$$a_p = \frac{\pi n_p {r_p}^2}{a} \tag{S5}$$

Porosity is similarly defined, but including the relevant lengths, with the total cylindrical pore volume related to the total membrane volume:

$$\varepsilon = \frac{\pi n_p {r_p}^2 L}{a \delta_m} = \frac{a_p L}{\delta_m} = a_p \tau \tag{S6}$$

Rearranging eq. S6:

$$a_p = \varepsilon / \tau \tag{S7}$$

Plugging eq. S7 into eq. S4 relates the water flux to capillary velocity, porosity, and tortuosity:

$$J_w = v\varepsilon / \tau \tag{S8}$$

The H-P equation for fully-developed, laminar flow through a cylinder relates the pressure drop to the average fluid velocity and the cylinder dimensions:

$$\Delta P = \frac{8 \mu v L}{{r_p}^2} = \frac{8 \mu v \delta_m \tau}{{r_p}^2} \tag{S9}$$

Finally, plugging eqs. S8 and S9 into eq. S3 yields eq. 1:

$$A = \frac{J_w}{\Delta P} = \frac{v\varepsilon \quad {r_p}^2}{\tau \; 8 \mu v \delta_m \tau} = \frac{\varepsilon r_p^2}{8 \tau^2 \mu \delta_m} \tag{1}$$

Conceptually, eq. S7 shows that increasing tortuosity will decrease the active pore area (and the corresponding number of pores) for a given volumetric porosity. By rearranging eq. S8, for a given water flux, the capillarity velocity v increases by a factor τ when compared to the axial velocity u, corresponding to the Epstein derivation. In other words, due to the decreased number of tortuous pores compared to vertical pores for a given porosity and pore radius, if the total water flux is equivalent, then the average capillary velocity in tortuous pores will be greater than that of vertical pores by a factor τ (*i.e.*, $v = u\tau$).

The above analysis ignores curvature, which is physically true for a straight cylindrical pore that is not vertically aligned, but does not accurately depict most other occurrences of tortuosity. Curvature has a complex impact on fluid flow, as reviewed by Berger *et al*. We can estimate the impact of curvature on fluid flow using the following series approximation:

$$\frac{Q_{\text{curve}}}{Q_{\text{straight}}} = 1 - 0.0306\left(\frac{K}{576}\right)^2 + 0.0120\left(\frac{K}{576}\right)^4 + \ldots \quad \text{(S10)}$$

where Q_{curve} is the flow rate through a coiled pipe, Q_{straight} is the flow rate under the same pressure gradient through a straight pipe with the same radius, and K is the Dean number:

$$K = \left(\frac{r_{\text{p}}}{R}\right)^{1/2} \frac{2 r_{\text{p}} v \rho}{\mu} \quad \text{(S11)}$$

where R is the radius of curvature, v is again the mean capillary velocity, and ρ is the fluid density. The Dean number relates inertial and centrifugal forces to the viscous force. Larger Dean numbers increase the impact of curvature on the flow rate, with K = 576 resulting in ~2% decreased flux.

To get a sense for the impact of curvature in block-polymer membranes, we can consider upper limits of water flow through block polymer membranes, with r_{p} = 50 nm, R = 250 nm, and v = 1000 μm/s. These values correspond to K = 0.00005, and essentially no change to the flow rate by eq. S10. In other words, the effects of curvature on fluid flow through tortuous pores in block polymer membranes should be negligible, and eq. 1 should be valid for the idealized model of tortuous capillaries of constant pore radius.

Table S1. Experimental water permeabilities and parameters used to calculate theoretical water permeability using the Hagen-Poiseuille equation

Pore Formation Mechanism	Experimental Permeability ($Lm^{-2}h^{-1}bar^{-1}$)	Average Pore Diameter (nm)	Porosity (%)	Active Layer Thickness (nm)	Theoretical Permeability ($Lm^{-2}h^{-1}bar^{-1}$)	Ref.
Etching	114	12.5	20	200	1975	1
Etching	1.2	24.2	27	4000	500	2
Etching	200	15	37	100	10,520	3
Etching	10	8	42	150	2265	4
Etching	153	13.2	38	1000	840	
Etching	4	12	45	800	1020	5
Etching	165	20	25	80	15,800	6
Etching	200	17	32	160	7300	7
Etching	97	15	24	100	6830	8
Etching	9	14	40	25,000	40	9
Etching	5	20	40	100,000	6830	10
Swelling	2000	35	11.7	85	2820	11
	8600	37	14	71	21,310	
	13,000	48.6	17.5	61	34,120	
	15,000	48.2	19.9	53	85,650	
Swelling	128	17.5	17.7	240	110,260	12
Swelling	5000	27	46	239	17,740	13
	2000	20	43	213	10,210	
Swelling	30	26	52	60,000	74	14
SNIPS	90.8	6.6	3.5	50	1540	15
SNIPS	60	12.5	12.7	1200	210	16
SNIPS	32	60.0	24.5	40	5570	17
SNIPS	24	8.0	7.4	100	600	18
	154	14.0	8.0	100	1980	
	196	14.0	7.6	100	1880	
	850	20.0	14.0	100	7080	
SNIPS	380	22.6	16.3	110	9400	19
SNIPS	750	20.0	10.0	100	5060	20
SNIPS	7.2	13.1	5.8	100	400	21
	310	16.2	14.3	100	4690	

SNIPS	13.4	13.1	11.2	100	2430	22
	20.1	9.0	4.0	100	410	
SNIPS	189	18.0	22.0	1400	640	23
	968	21.0	27.0	1400	1080	
	4650	28.0	33.0	800	4090	
SNIPS	262	25.6	10.6	106	7800	24
SNIPS	55	17.0	13.6	174	2890	25
	101	23.0	18.7	220	5680	
	1465	34.0	31.5	91	51,140	
SNIPS	150	21.0	5.0	2500	110	26
SNIPS	153	15.9	10.3	120	2740	27

Table S2. Experimental water permeabilities, BSA or PEO rejections, and ratio of BSA R_h to r_p for block polymer membranes

Pore Formation Mechanism	Experimental Permeability ($Lm^{-2}h^{-1}bar^{-1}$)	BSA or PEO Rejection (%)	λ	Ref.
Etching	165	22	0.37	28
Etching	1.2	20	0.31	2
Etching	196	22	0.73	6
Etching	150	80	0.61	
Swelling	1686	45	0.27	29
Swelling	104	38.4	0.36	30
	300	28.1	0.3	
	700	14.7	0.26	
	750	11.2	0.24	
	860	8.5	0.22	
	35	52	0.53	
	89	41	0.43	
	153	34	0.40	
	200	26	0.35	
	300	26	0.34	
Swelling	320	93	*	31
	840	81	*	
	960	78	*	
	1000	66	*	
	1100	50	*	
Swelling	1250	75	*	13
	1800	58	*	
	2100	35		
SNIPS	2.6	86	1.01	21
SNIPS	850	67	0.37	20
SNIPS	380	95	0.32	19
SNIPS	275	50	0.33	27
SNIPS	196	15	0.52	18
	24	85	0.9	

SNIPS	400	3	0.35	23
	200	5	0.41	
SNIPS	650	50	0.74	32
SNIPS	91	28	0.21	15
SNIPS	1150	12	0.42	33
	1100	20	0.42	
SNIPS	40	82	0.93	34
SNIPS	50	90	0.32	35
	240	17	0.17	
	390	5	0.11	

* Denotes that average pore size was not reported for these membranes.

Table S3. Average pore diameters and standard deviations used to calculate the pore size coefficient of variation for block polymer membranes

Pore Formation Mechanism	Average Pore Diameter (nm)	Standard Deviation (nm)	Coefficient of Variation	Ref.
Etching	25.0	3.0	0.12	28
Etching	20.3	3	0.15	36
Etching	20.0	3.0	0.15	2
Etching	15.0	2.6	0.17	8
Etching	12.0	1.3	0.11	5
Etching	17.0	2.4	0.14	7
Swelling	13.9	3.2	0.23	30
	18.4	3.8	0.207	
	21.2	4.3	0.203	
	24.4	5.0	0.205	
	27.7	6.8	0.245	
	33.4	8.2	0.246	
Swelling	20.0	4.0	0.2	13
	14.0	3.0	0.214	
	17.0	3.0	0.176	
Swelling	15.8	1.8	0.114	37
	19.5	2.0	0.103	
	22.1	3.3	0.149	
	22.8	2.6	0.114	
	23.4	2.0	0.085	
Swelling	8.0	2.0	0.25	12
	11.6	2.1	0.18	
	11.8	1.8	0.15	
	13.8	2.1	0.152	
	14.6	1.9	0.13	
	17.0	1.8	0.106	
	17.7	2.8	0.158	
Swelling	18.8	3.5	0.186	38
	25.3	3.1	0.123	
	35.8	5.6	0.156	

	40.0	4.4	0.11	
	44.1	4.4	0.11	
	52.9	2.7	0.05	
SNIPS	24.7	2.5	0.101	39
SNIPS	27.0	5.0	0.185	40
SNIPS	16.0	4.5	0.28	41
	21.0	4.5	0.21	
	20.0	7.5	0.38	
SNIPS	12.5	3.3	0.26	16
SNIPS	60.0	21	0.35	17
SNIPS	31.9	10.9	0.34	42
SNIPS	10.4	2.8	0.27	43
	18.0	4.0	0.22	
	15.8	5.0	0.32	
SNIPS	38.7	6.6	0.17	33
	32.1	7.1	0.22	
SNIPS	18.0	4.0	0.22	23
	28.0	12.0	0.43	
	41.0	14.0	0.34	
SNIPS	25.6	6.1	0.24	24
	42.6	17.9	0.42	
SNIPS	25.6	6.5	0.25	25
SNIPS	17.0	2.0	0.12	44
	23.0	2.0	0.09	
	53.0	5.0	0.1	
NIPS	38.8	18.4	0.47	45
	38.5	14.1	0.37	
	22.7	10.7	0.47	
	20.3	7.0	0.35	
	22.1	9.1	0.41	
	28.4	12.3	0.43	
	39.6	15.6	0.39	
	35.7	16.8	0.47	

Table S4. PEO-100k rejection (R_h ~ 10 nm) for block polymer membranes

Pore Formation Mechanism	Experimental Permeability ($Lm^{-2}h^{-1}bar^{-1}$)	PEO-100k Rejection (%)	Ref.
SNIPS	850	82	20
SNIPS	380	80	19
SNIPS	275	77	27
	153	95	
SNIPS	850	50	18
	196	90	
	154	95	
SNIPS	200	100	23
	400	80	
	1000	50	
	4500	40	
SNIPS	91	95	15
Etching	196	80	6
Etching	150	99	
Etching	165	99	28
Etching	1.2	93	2
Swelling	100	83	46
	560	85	
Swelling	460	90	47
	1200	70	
Swelling	750	99	48

References

(1) Zhou, H.-J.; Yang, G.-W.; Zhang, Y.-Y.; Xu, Z.-K.; Wu, G.-P. Bioinspired Block Copolymer for Mineralized Nanoporous Membrane. *ACS Nano* **2018**, *12* (11), 11471–11480. https://doi.org/10.1021/acsnano.8b06521.

(2) Phillip, W. A.; O'Neill, B.; Rodwogin, M.; Hillmyer, M. A.; Cussler, E. L. Self-Assembled Block Copolymer Thin Films as Water Filtration Membranes. *ACS Appl. Mater. Interfaces* **2010**, *2* (3), 847–853. https://doi.org/10.1021/am900882t.

(3) Seo, M.; Moll, D.; Silvis, C.; Roy, A.; Querelle, S.; Hillmyer, M. A. Interfacial Polymerization of Reactive Block Polymers for the Preparation of Composite Ultrafiltration Membranes. *Ind. Eng. Chem. Res.* **2014**, *53* (48), 18575–18579. https://doi.org/10.1021/ie5032259.

(4) Hampu, N.; Bates, M. W.; Vidil, T.; Hillmyer, M. A. Bicontinuous Porous Nanomaterials from Block Polymers Radically Cured in the Disordered State for Size-Selective Membrane Applications. *ACS Appl. Nano Mater.* **2019**. https://doi.org/10.1021/acsanm.9b00922.

(5) Hampu, N.; Hillmyer, M. A. Temporally Controlled Curing of Block Polymers in the Disordered State Using Thermally Stable Photoacid Generators for the Preparation of Nanoporous Membranes. *ACS Appl. Polym. Mater.* **2019**, *1* (5), 1148–1154. https://doi.org/10.1021/acsapm.9b00150.

(6) Vidil, T.; Hampu, N.; Hillmyer, M. A. Nanoporous Thermosets with Percolating Pores from Block Polymers Chemically Fixed above the Order–Disorder Transition. *ACS Cent. Sci.* **2017**. https://doi.org/10.1021/acscentsci.7b00358.

(7) Yang, S. Y.; Park, J.; Yoon, J.; Ree, M.; Jang, S. K.; Kim, J. K. Virus Filtration Membranes Prepared from Nanoporous Block Copolymers with Good Dimensional Stability under High Pressures and Excellent Solvent Resistance. *Advanced Functional Materials* **2008**, *18* (9), 1371–1377. https://doi.org/10.1002/adfm.200700832.

(8) Jackson, E. A.; Lee, Y.; Hillmyer, M. A. ABAC Tetrablock Terpolymers for Tough Nanoporous Filtration Membranes. *Macromolecules* **2013**, *46* (4), 1484–1491. https://doi.org/10.1021/ma302414w.

(9) Li, L.; Szewczykowski, P.; Clausen, L. D.; Hansen, K. M.; Jonsson, G. E.; Ndoni, S. Ultrafiltration by Gyroid Nanoporous Polymer Membranes. *Journal of Membrane Science* **2011**, *384* (1), 126–135. https://doi.org/10.1016/j.memsci.2011.09.012.

(10) Phillip, W. A.; Amendt, M.; O'Neill, B.; Chen, L.; Hillmyer, M. A.; Cussler, E. L. Diffusion and Flow Across Nanoporous Polydicyclopentadiene-Based Membranes. *ACS Appl. Mater. Interfaces* **2009**, *1* (2), 472–480. https://doi.org/10.1021/am8001428.

(11) Guo, L.; Wang, L.; Wang, Y. Stretched Homoporous Composite Membranes with Elliptic Nanopores for External-Energy-Free Ultrafiltration. *Chem. Commun.* **2016**, *52* (42), 6899–6902. https://doi.org/10.1039/C6CC01353H.

(12) Ahn, H.; Park, S.; Kim, S.-W.; Yoo, P. J.; Ryu, D. Y.; Russell, T. P. Nanoporous Block Copolymer Membranes for Ultrafiltration: A Simple Approach to Size Tunability. *ACS Nano* **2014**, *8* (11), 11745–11752. https://doi.org/10.1021/nn505234v.

(13) Yao, X.; Guo, L.; Chen, X.; Huang, J.; Steinhart, M.; Wang, Y. Filtration-Based Synthesis of Micelle-Derived Composite Membranes for High-Flux Ultrafiltration. *ACS Appl. Mater. Interfaces* **2015**, *7* (12), 6974–6981. https://doi.org/10.1021/acsami.5b01004.

(14) Wang, Z.; Liu, R.; Yang, H.; Wang, Y. Nanoporous Polysulfones with *in Situ* PEGylated Surfaces by a Simple Swelling Strategy Using Paired Solvents. *Chem. Commun.* **2017**, *53* (65), 9105–9108. https://doi.org/10.1039/C7CC04091A.

(15) Liu, Y.; Liu, T.; Su, Y.; Yuan, H.; Hayakawa, T.; Wang, X. Fabrication of a Novel PS4VP/PVDF Dual-Layer Hollow Fiber Ultrafiltration Membrane. *Journal of Membrane Science* **2016**, *506*, 1–10. https://doi.org/10.1016/j.memsci.2016.01.047.

(16) Bucher, T.; Filiz, V.; Abetz, C.; Abetz, V. Formation of Thin, Isoporous Block Copolymer Membranes by an Upscalable Profile Roller Coating Process—A Promising Way to Save Block Copolymer. *Membranes* **2018**, *8* (3). https://doi.org/10.3390/membranes8030057.

(17) Zhang, Y.; Mulvenna, R. A.; Boudouris, B. W.; Phillip, W. A. Nanomanufacturing of High-Performance Hollow Fiber Nanofiltration Membranes by Coating Uniform Block Polymer Films from Solution. *J. Mater. Chem. A* **2017**, *5* (7), 3358–3370. https://doi.org/10.1039/C6TA09287J.

(18) Dorin, R. M.; Phillip, W. A.; Sai, H.; Werner, J.; Elimelech, M.; Wiesner, U. Designing Block Copolymer Architectures for Targeted Membrane Performance. *Polymer* **2014**, *55* (1), 347–353. https://doi.org/10.1016/j.polymer.2013.09.038.

(19) Pendergast, M. M.; Mika Dorin, R.; Phillip, W. A.; Wiesner, U.; Hoek, E. M. V. Understanding the Structure and Performance of Self-Assembled Triblock Terpolymer Membranes. *Journal of Membrane Science* **2013**, *444*, 461–468. https://doi.org/10.1016/j.memsci.2013.04.074.

(20) Karunakaran, M.; Nunes, S. P.; Qiu, X.; Yu, H.; Peinemann, K.-V. Isoporous PS-B-PEO Ultrafiltration Membranes *via* Self-Assembly and Water-Induced Phase Separation. *Journal of Membrane Science* **2014**, *453*, 471–477. https://doi.org/10.1016/j.memsci.2013.11.015.

(21) Zhu, G.; Ying, Y.; Li, X.; Liu, Y.; Yang, C.; Yi, Z.; Gao, C. Isoporous Membranes with Sub-10 Nm Pores Prepared from Supramolecular Interaction Facilitated Block Copolymer Assembly and Application for Protein Separation. *Journal of Membrane Science* **2018**, *566*, 25–34. https://doi.org/10.1016/j.memsci.2018.08.033.

(22) Zhu, G.-D.; Yang, C.-Y.; Yin, Y.-R.; Yi, Z.; Chen, X.-H.; Liu, L.-F.; Gao, C.-J. Preparation of Isoporous Membranes from Low χ Block Copolymers *via* Co-Assembly with H-Bond Interacting Homopolymers. *Journal of Membrane Science* **2019**, *589*, 117255. https://doi.org/10.1016/j.memsci.2019.117255.

(23) Gu, Y.; Wiesner, U. Tailoring Pore Size of Graded Mesoporous Block Copolymer Membranes: Moving from Ultrafiltration toward Nanofiltration. *Macromolecules* **2015**, *48* (17), 6153–6159. https://doi.org/10.1021/acs.macromol.5b01296.

(24) Schöttner, S.; Brodrecht, M.; Uhlein, E.; Dietz, C.; Breitzke, H.; Tietze, A. A.; Buntkowsky, G.; Gallei, M. Amine-Containing Block Copolymers for the Bottom-Up Preparation of Functional Porous Membranes. *Macromolecules* **2019**, *52* (7), 2631–2641. https://doi.org/10.1021/acs.macromol.8b02758.

(25) Shevate, R.; Kumar, M.; Cheng, H.; Hong, P.-Y.; Behzad, A. R.; Anjum, D.; Peinemann, K.-V. Rapid Size-Based Protein Discrimination inside Hybrid Isoporous Membranes. *ACS Appl. Mater. Interfaces* **2019**, *11* (8), 8507–8516. https://doi.org/10.1021/acsami.8b20802.

(26) Gu, Y.; Dorin, R. M.; Wiesner, U. Asymmetric Organic–Inorganic Hybrid Membrane Formation *via* Block Copolymer–Nanoparticle Co-Assembly. *Nano Lett.* **2013**, *13* (11), 5323–5328. https://doi.org/10.1021/nl402829p.

(27) Phillip, W. A.; Dorin, R. M.; Werner, J.; Hoek, E. M. V.; Wiesner, U.; Elimelech, M. Tuning Structure and Properties of Graded Triblock Terpolymer-Based Mesoporous and Hybrid Films. *Nano Lett.* **2011**, *11* (7), 2892–2900. https://doi.org/10.1021/nl2013554.

(28) Querelle, S. E.; Jackson, E. A.; Cussler, E. L.; Hillmyer, M. A. Ultrafiltration Membranes with a Thin Poly(styrene)-B-Poly(isoprene) Selective Layer. *ACS Appl. Mater. Interfaces* **2013**, *5* (11), 5044–5050. https://doi.org/10.1021/am400847m.

(29) Sun, W.; Wang, Z.; Yao, X.; Guo, L.; Chen, X.; Wang, Y. Surface-Active Isoporous Membranes Nondestructively Derived from Perpendicularly Aligned Block Copolymers for Size-Selective Separation. *Journal of Membrane Science* **2014**, *466*, 229–237. https://doi.org/10.1016/j.memsci.2014.04.055.
(30) Shi, X.; Wang, Z.; Wang, Y. Highly Permeable Nanoporous Block Copolymer Membranes by Machine-Casting on Nonwoven Supports: An Upscalable Route. *Journal of Membrane Science* **2017**, *533*, 201–209. https://doi.org/10.1016/j.memsci.2017.03.046.
(31) Yan, N.; Wang, Z.; Wang, Y. Highly Permeable Membranes Enabled by Film Formation of Block Copolymers on Water Surface. *Journal of Membrane Science* **2018**, *568*, 40–46. https://doi.org/10.1016/j.memsci.2018.09.047.
(32) Xie, Y.; Moreno, N.; Calo, V. M.; Cheng, H.; Hong, P.-Y.; Sougrat, R.; Behzad, A. R.; Tayouo, R.; Nunes, S. P. Synthesis of Highly Porous Poly(tert-Butyl Acrylate)-B-Polysulfone-B-Poly(tert-Butyl Acrylate) Asymmetric Membranes. *Polym. Chem.* **2016**, *7* (18), 3076–3089. https://doi.org/10.1039/C6PY00215C.
(33) Shevate, R.; Kumar, M.; Karunakaran, M.; Hedhili, M. N.; Peinemann, K.-V. Polydopamine/Cysteine Surface Modified Isoporous Membranes with Self-Cleaning Properties. *Journal of Membrane Science* **2017**, *529*, 185–194. https://doi.org/10.1016/j.memsci.2017.01.058.
(34) Peinemann, K.-V.; Abetz, V.; Simon, P. F. W. Asymmetric Superstructure Formed in a Block Copolymer *via* Phase Separation. *Nature Materials* **2007**, *6*, 992.
(35) Rangou, S.; Buhr, K.; Filiz, V.; Clodt, J. I.; Lademann, B.; Hahn, J.; Jung, A.; Abetz, V. Self-Organized Isoporous Membranes with Tailored Pore Sizes. *Journal of Membrane Science* **2014**, *451*, 266–275. https://doi.org/10.1016/j.memsci.2013.10.015.
(36) Vriezekolk, E. J.; Kudernac, T.; de Vos, W. M.; Nijmeijer, K. Composite Ultrafiltration Membranes with Tunable Properties Based on a Self-Assembling Block Copolymer/homopolymer System. *Journal of Polymer Science Part B: Polymer Physics* **2015**, *53* (21), 1546–1558. https://doi.org/10.1002/polb.23795.
(37) Guo, L.; Wang, Z.; Wang, Y. Perpendicular Alignment and Selective Swelling-Induced Generation of Homopores of Polystyrene-B-poly(2-Vinylpyridine)-B-Poly(ethylene Oxide) Triblock Terpolymer. *Macromolecules* **2018**, *51* (16), 6248–6256. https://doi.org/10.1021/acs.macromol.8b01358.
(38) Yin, J.; Yao, X.; Liou, J.-Y.; Sun, W.; Sun, Y.-S.; Wang, Y. Membranes with Highly Ordered Straight Nanopores by Selective Swelling of Fast Perpendicularly Aligned Block Copolymers. *ACS Nano* **2013**, *7* (11), 9961–9974. https://doi.org/10.1021/nn403847z.
(39) Schöttner, S.; Schaffrath, H.-J.; Gallei, M. Poly(2-Hydroxyethyl Methacrylate)-Based Amphiphilic Block Copolymers for High Water Flux Membranes and Ceramic Templates. *Macromolecules* **2016**, *49* (19), 7286–7295. https://doi.org/10.1021/acs.macromol.6b01803.
(40) Dami, S.; Abetz, C.; Fischer, B.; Radjabian, M.; Georgopanos, P.; Abetz, V. A Correlation between Structural Features of an Amphiphilic Diblock Copolymer in Solution and the Structure of the Porous Surface in an Integral Asymmetric Membrane. *Polymer* **2017**, *126*, 376–385. https://doi.org/10.1016/j.polymer.2017.05.024.

(41) Hahn, J.; Clodt, J. I.; Abetz, C.; Filiz, V.; Abetz, V. Thin Isoporous Block Copolymer Membranes: It Is All about the Process. *ACS Appl. Mater. Interfaces* **2015**, *7* (38), 21130–21137. https://doi.org/10.1021/acsami.5b04658.
(42) Shevate, R.; Karunakaran, M.; Kumar, M.; Peinemann, K.-V. Polyanionic pH-Responsive Polystyrene-B-poly(4-Vinyl Pyridine-N-Oxide) Isoporous Membranes. *Journal of Membrane Science* **2016**, *501*, 161–168. https://doi.org/10.1016/j.memsci.2015.11.038.
(43) Li, Y. M.; Zhang, Q.; Álvarez-Palacio, J. R.; Hakem, I. F.; Gu, Y.; Bockstaller, M. R.; Wiesner, U. Effect of Humidity on Surface Structure and Permeation of Triblock Terpolymer Derived SNIPS Membranes. *Polymer* **2017**, *126*, 368–375. https://doi.org/10.1016/j.polymer.2017.05.037.
(44) Hahn, J.; Clodt, J. I.; Filiz, V.; Abetz, V. Protein Separation Performance of Self-Assembled Block Copolymer Membranes. *RSC Adv.* **2014**, *4* (20), 10252–10260. https://doi.org/10.1039/C3RA47306F.
(45) Tiraferri, A.; Yip, N. Y.; Phillip, W. A.; Schiffman, J. D.; Elimelech, M. Relating Performance of Thin-Film Composite Forward Osmosis Membranes to Support Layer Formation and Structure. *Journal of Membrane Science* **2011**, *367* (1), 340–352. https://doi.org/10.1016/j.memsci.2010.11.014.
(46) Wang, Z.; Guo, L.; Wang, Y. Isoporous Membranes with Gradient Porosity by Selective Swelling of UV-Crosslinked Block Copolymers. *Journal of Membrane Science* **2015**, *476*, 449–456. https://doi.org/10.1016/j.memsci.2014.12.009.
(47) Wang, Z.; Wang, Y. Highly Permeable and Robust Responsive Nanoporous Membranes by Selective Swelling of Triblock Terpolymers with a Rubbery Block. *Macromolecules* **2016**, *49* (1), 182–191. https://doi.org/10.1021/acs.macromol.5b02275.
(48) Ma, D.; Zhou, J.; Wang, Z.; Wang, Y. Block Copolymer Ultrafiltration Membranes by Spray Coating Coupled with Selective Swelling. *Journal of Membrane Science* **2020**, *598*, 117656. https://doi.org/10.1016/j.memsci.2019.117656.